THE ASTRONOMICAL JOURNAL, 121:2781–2791, 2001 May
© 2001. The American Astronomical Society. All rights reserved. Printed in U.S.A.

NEAR-INFRARED SPECTROSCOPY OF THE CASSIOPEIA A AND KEPLER SUPERNOVA REMNANTS

CHRISTOPHER L. GERARDY AND ROBERT A. FESEN
Department of Physics and Astronomy, 6127 Wilder Laboratory, Dartmouth College, Hanover, NH 03755-3528
Received 2000 November 6; accepted 2001 January 22

ABSTRACT

Near-infrared spectra (0.95–2.4 μm) of the Cassiopeia A and Kepler supernova remnants (SNRs) are presented. Low-dispersion ($R \approx 700$) spectra were obtained for five bright fast-moving ejecta knots (FMKs) at two locations on the main shell and for three bright circumstellar knots (quasi-stellar flocculi or QSFs) near the southwest rim of Cas A. The main shell FMKs in Cas A exhibit a sparse near-infrared spectrum dominated by [S II] 1.03 μm emission with a handful of other, fainter emission lines. Among these are two high-ionization silicon lines, [Si VI] 1.96 and [Si X] 1.43 μm, which have been detected in active galactic nuclei and novae but never before in a supernova remnant. The near-infrared spectra of circumstellar QSFs in Cas A show a much richer spectrum, with strong He I 1.083 μm emission and over a dozen bright [Fe II] lines. Observed [Fe II] line ratios indicate electron densities of 5–9 $\times$ 10^4 cm^{-3} in the QSFs. The Cas A QSF data are quite similar to the observed spectrum of a bright circumstellar knot along the northwest rim of the Kepler SNR, which also shows strong He I and [Fe II] emission with a measured electron density of 2.5–3 $\times$ 10^4 cm^{-3}. Finally, we present *J*- and *K*-band images of Cas A. The *K*-band image shows faint diffuse emission that has no optical or mid-infrared counterpart but is morphologically similar to radio continuum maps and may be infrared synchrotron radiation.

Key words: circumstellar matter — infrared radiation — ISM: individual (Cassiopeia A, Kepler's supernova remnant) — ISM: lines and bands — supernova remnants

1. INTRODUCTION

The numerous optical and UV spectroscopic studies of supernova remnants (SNRs) in the literature have resulted in a rich catalog of observed emission-line features (cf. Fesen & Hurford 1996 and references therein). However, most of these studies do not extend much beyond 8500 Å because of the poor sensitivity of optical detectors further to the red. Only a handful of published SNR spectra go out as far as 1.1 μm, where the most commonly seen features are [S III] 9069, 9532 Å, [C I] 9823, 9850 Å, [S II] 10287–10372 Å, and He I 10830 Å (e.g., Dennefeld & Andrillat 1981; Dennefeld 1982; Henry, MacAlpine, & Kirshner 1984).

With the maturing of high quantum efficiency near-infrared (NIR) detectors, it is now possible to probe the spectra of SNRs in the 1–5 μm wavelength regime, and there are a number of reasons to do so. Near-infrared spectroscopy can provide access to features that are not available in optical and UV spectra, such as molecular species like H_2 and CO, which can provide valuable information about molecule formation and destruction in SNRs. Molecular emission can also often be used as an astrophysical probe, providing information about temperature, density, and excitation mechanisms. In addition, there are many strong lines of [Fe II] in the NIR that can be used as density diagnostics. These lines have higher critical densities than optical density–sensitive lines and thus can probe much higher densities ($\sim 10^3$–10^5 cm^{-3}). Finally, the near-infrared contains several strong high-ionization species that have been seen in other objects such as active galactic nuclei (AGNs), novae, and planetary nebulae. These lines could provide important information about ionization processes and structures in supernova remnants.

Unfortunately, few NIR spectra of supernova remnants currently exist in the literature. Furthermore, there are almost no near-infrared data that take advantage of large-format array detectors allowing for spatially resolved long-slit spectroscopy and broad wavelength coverage. Indeed, of the few data sets available, most were obtained with relatively large apertures ($\sim 5''$– $20''$) in narrow wavelength regions typically covering only a single emission feature with each bandpass.

To date, the most comprehensive work on the NIR spectra of supernova remnants has been the study of molecular hydrogen (H_2) emission from shocks running into molecular clouds. This has been seen in IC 443, RCW 103, and the Cygnus Loop (Treffers 1979; Graham, Wright, & Longmore 1987; Oliva, Moorwood, & Danziger 1989, hereafter OMD89; Oliva, Moorwood, & Danziger 1990, hereafter OMD90; Burton & Spiromilio 1993; Graham et al. 1991; Graham, Wright, & Geballe 1991; Richter, Graham, & Wright 1995). H_2 has also been detected in the Crab Nebula (Graham, Wright, & Longmore 1990), presumably from dense, neutral cores of the emission-line filaments.

Other near-infrared work on SNRs has focused on [Fe II] line emission, which is typically 2 orders of magnitude brighter, relative to H I, than that seen in H II regions (Seward et al. 1983; OMD89). The large [Fe II]/H I ratios observed have been suggested as a good tracer for shocks in extragalactic studies (e.g., OMD89), and near-infrared [Fe II] imaging has been used to probe extragalactic SNR populations (e.g., Greenhouse et al. 1997). However, a large [Fe II]/H I ratio is not always an indication of shocks as the strong [Fe II] emission seen in the Crab Nebula is likely a result of photoionization (Graham et al. 1990). Also, relative NIR [Fe II] line ratios have been used to deduce electron densities for Kepler, N63A, N49, N103B (OMD89), RCW 103 (OMD89; OMD90), and the Crab Nebula (Rudy, Rossano, & Puetter 1994).

In this paper, we present 0.95–2.4 μm spectra of shocked, metal-rich ejecta in the Cassiopeia A (Cas A) supernova

remnant, as well as J- and K-band images. To our knowledge, these are the first published NIR spectra of a young, "oxygen-rich" supernova remnant. We also present NIR spectra of shocked circumstellar mass-loss material, both in Cas A and in Kepler's SNR.

2. OBSERVATIONS AND DATA REDUCTION

Low-dispersion near-infrared spectroscopy and imaging of the Cas A and Kepler supernova remnants were obtained with the 2.4 m Hiltner telescope at MDM Observatory on the southwest ridge of Kitt Peak in Arizona. Spectroscopic observations of Cas A took place in late November and early December of 1999. J- and K-band images of Cas A were obtained in 2000 November. Kepler's SNR was observed in 2000 April.

All observations were obtained with TIFKAM (also known as ONIS), a high-throughput infrared imager and spectrograph with an ALLADIN 512 × 1024 InSb detector. This instrument can be operated with standard J, H, and K filters for broadband imaging, or with a variety of grisms, blocking filters, and an east-west oriented 0.″6 slit, allowing low ($R \approx 700$) and moderate ($R \approx 1400$) resolution spectroscopic observations from 0.95 to 2.5 μm.

J- and K-band imaging of Cas A was performed using the following procedure: Sets of four dithered 30 s on-target images were immediately followed by four dithered 30 s images of fields $\approx 10'$ off-target. The off-target images were averaged together with high-pixel rejection to remove stars, creating sky background images that were then subtracted from the on-target images. This process was repeated four times for each on-target pointing. The entire remnant was covered in several overlapping positions, resulting in total on-target integration times of 32–64 minutes in K band and 24–48 minutes in J band. Sky-subtracted on-target images were registered and combined using standard IRAF tasks. J-band imaging of the Kepler SNR was performed in a similar manner, but with only one on-target position and 8 minutes total on-target integration time.

Near-infrared 0.95–2.4 μm long-slit spectra of Cas A and Kepler were obtained using three spectroscopic setups covering the 0.95–1.8, 1.2–2.2, and 2.0–2.4 μm wavelength regions. In Cas A, five metal-rich ejecta knots, or fast-moving knots (FMKs), were observed at two slit positions on the main shell, and three bright knots of circumstellar mass-loss material, or quasi-stationary flocculi (QSFs), were observed near the southwest rim of the remnant. The Kepler SNR was observed at a single position on the northwest rim, the region with the brightest optical emission. The spectroscopically observed regions of Cas A and Kepler are marked on the J-band images shown in Figures 1 and 2.

Table 1 lists the log of spectroscopic exposures for each slit position. Between on-target exposures the telescope was dithered along the slit to sample the array at multiple locations. For sufficiently isolated knots (QSF 1, QSF 3, and Kepler), dithered on-target exposures were used for first-order night-sky subtraction. For the other regions (QSF 2 and the FMKs), night-sky spectra were obtained between on-target exposures by observing an empty location 10′ north of the remnant and then removed from the on-target data. Figures 3 and 4 show representative two-dimensional long-slit spectra of FMKs 1 and 2 and QSF 1 in Cas A. Each frame shown is a single 900 s exposure in a single spectroscopic setup after first-order night-sky subtraction has been performed. One-dimensional spectra were extracted from these two-dimensional frames using standard IRAF tasks. Arc lamps were observed at each telescope position to provide wavelength calibration.

TABLE 1

LOG OF OBSERVATIONS

Bandpass (μm)	Exposure (s)
FMK 1 and 2	
0.95–1.8.....	7 × 900
1.2–2.2	3 × 900
2.0–2.4	2 × 900
FMK 3, 4, and 5	
0.95–1.8.....	6 × 900
1.2–2.2	3 × 900
QSF 1	
0.95–1.8.....	5 × 900
1.2–2.2	3 × 900
2.0–2.4	6 × 900
QSF 2	
0.95–1.8.....	3 × 900
1.2–2.2	7 × 900
2.0–2.4	3 × 900
QSF 3	
0.95–1.8.....	3 × 900
1.2–2.2	3 × 900
2.0–2.4	3 × 900
Kepler	
0.95–1.8.....	10 × 900
1.2–2.2	5 × 900

The spectra were corrected for telluric absorption by observing nearby A stars and early G dwarfs from the Bright Star Catalog (Hoffleit & Jaschek 1982). Applying the procedure described by Hanson, Rieke, & Luhman (1998), hereafter HRL98, stellar features were removed from the G dwarf spectra by dividing by a normalized solar spectrum (Livingston & Wallace 1991; Wallace, Hinkle, & Livingston 1993).[1] The resulting spectra were used to correct for telluric absorption in the A stars. The hydrogen features in the corrected A star spectra were removed from the raw A star spectra, and the results were used to correct the target data for telluric absorption. (For further discussion of this procedure see HRL98; Hanson, Conti, & Rieke 1996, and references therein.) The instrumental response was calibrated by matching the continuum of the A star telluric standards to the stellar atmosphere models of Kurucz (1994).

After correction for instrumental response and telluric absorption, the data for each knot in a given spectroscopic setup were averaged together. Data taken with different setups were then flux-matched in the overlapping wavelength regions and joined together to make a single full-coverage one-dimensional spectrum. Three Massey & Gronwall (1990) spectrophotometric standards were observed to set the absolute flux levels. The resulting abso-

[1] National Solar Observatory Kitt Peak Fourier Transform Spectroscope data used here were produced by NSF/NOAO.

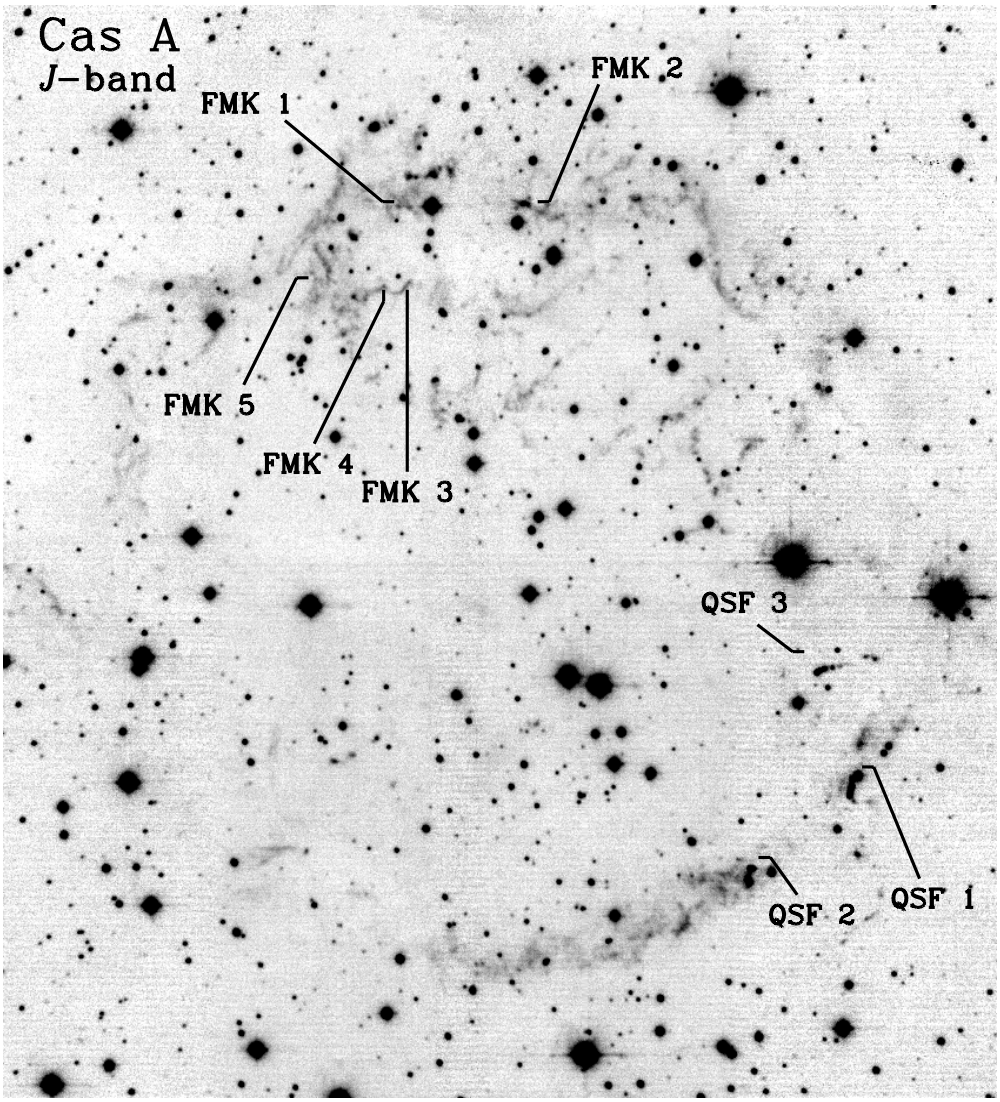


FIG. 1.—*J*-band image of Cas A with the locations of the observed FMKs and QSFs marked. North is up and east is to the left.

lute flux calibration is believed accurate to $\simeq 20\%$ shortward of 1.8 μm and $\simeq 30\%$ from 1.8 to 2.4 μm.

3. RESULTS AND DISCUSSION

Observed spectra of FMK 1 and QSF 1 in Cas A are presented in Figures 5 and 6, respectively, with the spectrum of the west rim of the Kepler SNR shown in Figure 7. Line identifications for the Cas A FMK spectra are presented in Table 2 (FMKs 1 and 2) and Table 3 (FMKs 3, 4, and 5), along with measured line centers and line fluxes, both observed and dereddened. Table 4 shows the line identifications and observed and dereddened fluxes for the Cas A QSFs and the western knot in Kepler. All wavelengths are given as vacuum values. Dereddening of the observed spectra was performed using the extinction curve of Cardelli, Clayton, & Mathis (1989). For the Cas A data, $E(B-V) = 1.5$ was used although the actual extinction varies significantly across the remnant (Hurford & Fesen 1996, hereafter HF96). For the Kepler data, we assumed $E(B-V) = 0.9$ (Blair, Long, & Vancura 1991)

3.1. *Cas A FMK Spectra*

Optical spectra of Cas A ejecta knots (FMKs) exhibit strong forbidden oxygen and sulfur emission and contain a number of fainter metal lines. These spectra show no indication of H or He, and little, if any, [Fe II] emission (HF96). (Complete 4000–10500 Å optical spectra of FMKs 1 and 2 are presented by HF96.) The near-infrared spectra of Cas A FMKs are intrinsically faint compared with their optical emission, and they are dominated by the [S II] 1.03 μm blend. A handful of other faint, low-ionization forbidden lines are seen including [C I] 0.9827, 0.9853, [P II] 1.1471, 1.1886, and [Fe II] 1.2570 and 1.6440 μm. We note that the 1.6440 μm feature could be blended with [Si I] 1.646 μm emission. In FMK 2, the brightest FMK we observed in Cas A, three other faint [Fe II] lines (1.2791, 1.2946, and 1.3209 μm) were weakly detected. Two other weak lines near 1.08 and 1.13 μm could be emission from the [S I] ^3P–^1D doublet but could also be due to (or blended with) He I 1.083 and O I 1.129 μm. O I emission would be consistent with the presence of weak permitted O I lines seen in the optical spectra of Cas A FMKs (e.g., HF96).

Perhaps the most interesting near-infrared lines detected in the brighter FMKs (1, 2, and 4) are those near the rest wavelengths of 1.43 and 1.96 μm. We identify these as high-ionization lines of silicon, [Si VI] 1.965 and [Si X] 1.4305 μm. The detection of such high-ionization species was unexpected as no other high-ionization lines are observed in

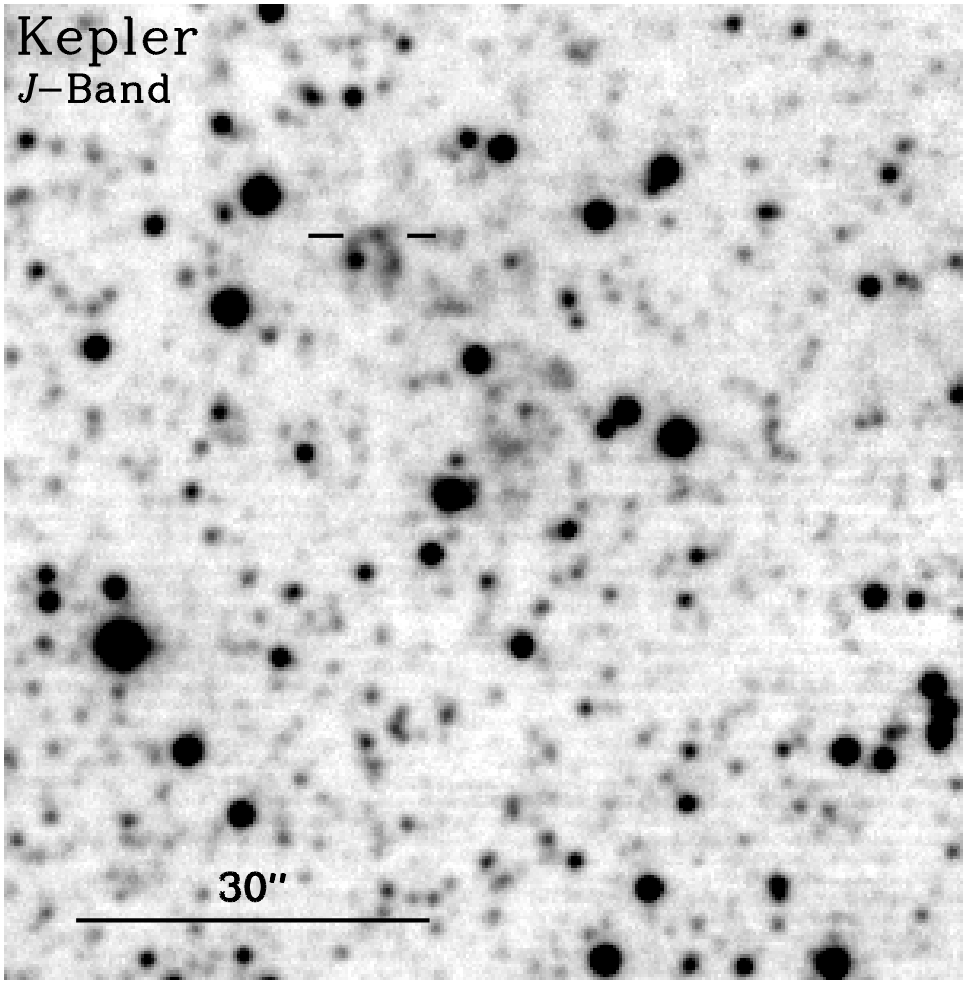


FIG. 2.—*J*-band image of Kepler with the location of the observed circumstellar knot marked. North is up and east is to the left.

TABLE 2

LINE IDENTIFICATIONS FOR FMKS 1 AND 2

		FMK 1			FMK 2		
λ_{lab} (μm)	LINE ID	λ_{obs} (μm)	$I(\lambda)$	$F(\lambda)$[a]	λ_{obs} (μm)	$I(\lambda)$	$F(\lambda)$[a]
0.9827, 0.9853	[C I] $^3P_{1,2}$–$^1D_2$	0.979	31	253	0.981	58	349
1.0290, 1.0323, 1.0339, 1.0373.....	[S II] $^2D_{5/2,3/2}$–$^2P_{3/2,1/2}$	1.028	1280	6650	1.027	3090	11600
1.0824	[S I] $^3P_2$–$^1D_2$	1.078	54	250	1.079	228	1043
1.0832	He I $^3S_1$–$^3P_{0,1,2}$	...	...	...	...	...	...
1.1289, 1.1290	O I $^3P_{0,1,2}$–$^3D_{1,2,3}$	1.125	33	139	1.125	55	238
1.1309	[S I] $^3P_1$–$^1D_2$	...	...	...	...	...	...
1.1471	[P II] $^3P_1$–$^1D_2$	1.143	20	79	1.142	39	160
1.1886	[P II] $^3P_2$–$^1D_2$	1.184	50	186	1.183	103	375
1.2570	[Fe II] $a^6D_{9/2}$–$a^4D_{7/2}$	1.251	37	120	1.254	76	253
1.2791	[Fe II] $a^6D_{3/2}$–$a^4D_{3/2}$	...	...	...	1.279	21	67
1.2946	[Fe II] $a^6D_{5/2}$–$a^4D_{5/2}$	...	...	...	1.293	23	66
1.3209	[Fe II] $a^6D_{7/2}$–$a^4D_{7/2}$	...	...	...	1.319	17	50
1.4305	[Si X] $^2P_{1/2}$–$^2P_{3/2}$	1.425	35	93	1.424	76	111
1.6440	[Fe II] $a^4F_{9/2}$–$a^4D_{7/2}$	1.639	27	59	1.638	54	118
1.6459	[Si I] $^3P_2$–$^1D_2$	...	...	...	...	...	...
1.965	[Si VI] $^2P_{3/2}$–$^2P_{2/2}$	1.955	69	124	1.952	268	480

NOTE.—Line fluxes are in units of 10^{-15} erg s^{-1} cm^{-2}.

[a] Corrected for $E(B-V) = 1.5$.

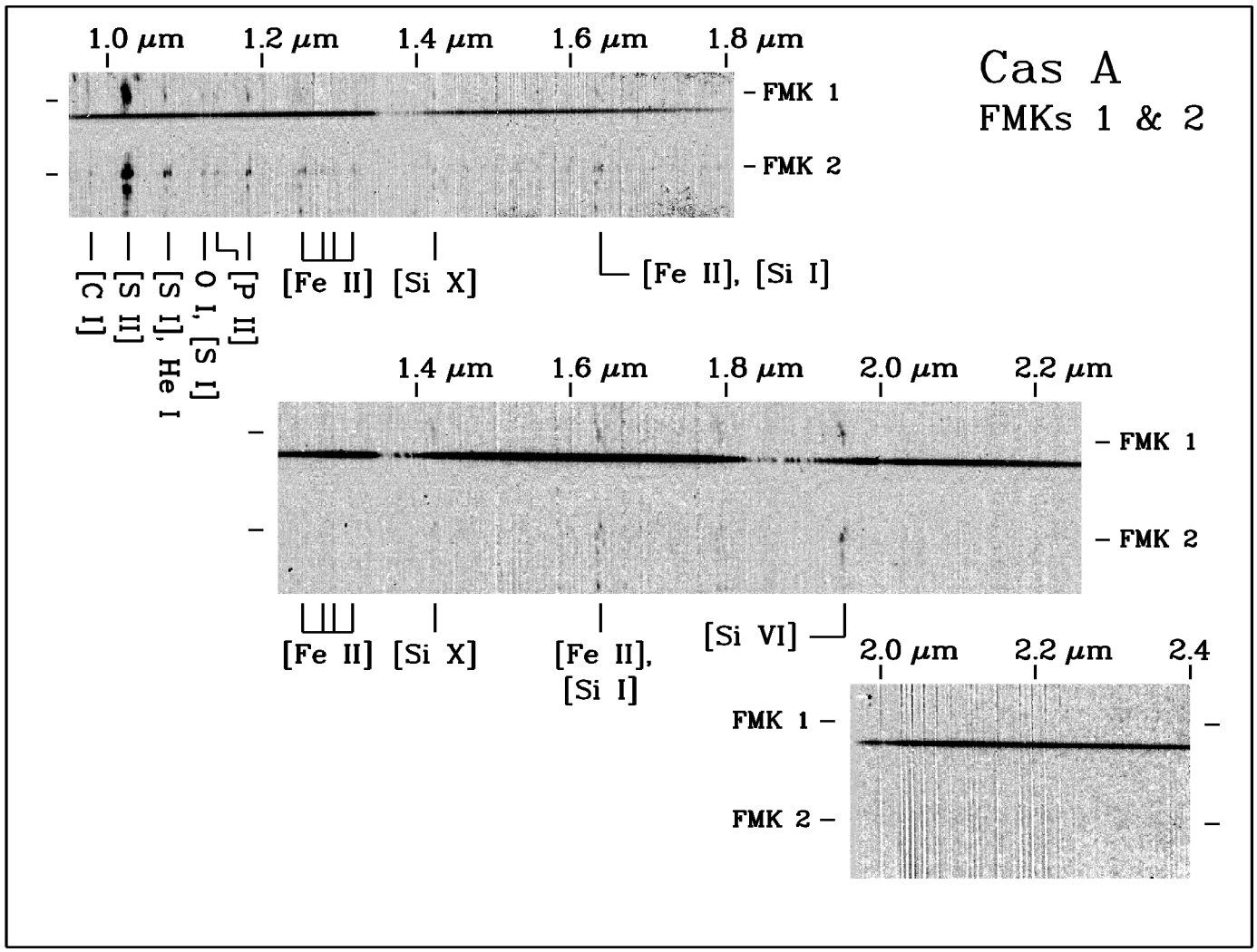


FIG. 3.—Two-dimensional long-slit spectra of Cas A FMKs 1 and 2. Each frame shows a single 900 s exposure from a spectroscopic setup. Full 0.95–2.4 μm coverage was achieved with three overlapping spectroscopic setups. First-order removal of night-sky lines has been performed, but the data shown are not corrected for telluric absorption or instrumental response. The approximate wavelength scale (in micron) is marked along the top of each frame, and the positions of the various observed features are shown at the bottom. Lines at the left and right of each frame in Fig. 3 denote the ends of the one-dimensional extraction apertures.

TABLE 3

LINE IDENTIFICATIONS FOR FMKs 3, 4, AND 5

		FMK 3			FMK 4			FMK 5		
λ_{lab} (μm)	LINE ID	λ_{obs} (μm)	$I(\lambda)$	$F(\lambda)$[a]	λ_{obs} (μm)	$I(\lambda)$	$F(\lambda)$[a]	λ_{obs} (μm)	$I(\lambda)$	$F(\lambda)$[a]
0.9827, 0.9853	[C I] $^3P_{1,2}$–$^1D_2$	0.977	22	128	0.978	51	306	…	…	…
1.0290, 1.0323, 1.0339, 1.0373,	[S II] $^2D_{5/2,3/2}$–$^2P_{3/2,1/2}$	1.025	464	2450	1.025	412	2210	1.044	156	784
1.0824	[S I] $^3P_2$–$^1D_2$	1.075	41	186	1.075	30	139	1.096	15	61
1.0832	He I $^3S_1$–$^3P_{0,1,2}$	…	…	…	…	…	…	…	…	…
1.1289, 1.1290	O I $^3P_{0,1,2}$–$^3D_{1,2,3}$	1.122	31	135	1.122	25	106	1.144	6	24
1.1309	[S I] $^3P_1$–$^1D_2$	…	…	…	…	…	…	…	…	…
1.1886	[P II] $^3P_2$–$^1D_2$	1.180	19	70	1.181	23	87	1.202	11	39
1.2570	[Fe II] $a^6D_{9/2}$–$a^4D_{7/2}$	1.248	16	57	1.248	16	60	1.271	20	64
1.4305	[Si X] $^2P_{1/2}$–$^2P_{3/2}$	…	…	…	1.420	16	40	…	…	…
1.6440	[Fe II] $a^4F_{9/2}$–$a^4D_{7/2}$	1.632	14	30	1.633	20	43	1.663	20	44
1.6459	[Si I] $^3P_2$–$^1D_2$	…	…	…	…	…	…	…	…	…
1.965	[Si VI] $^2P_{3/2}$–$^2P_{2/2}$	…	…	…	1.951	20	36	…	…	…

NOTE.—Line fluxes are in units of 10^{-15} erg s^{-1} cm^{-2}.

[a] Corrected for $E(B-V) = 1.5$.

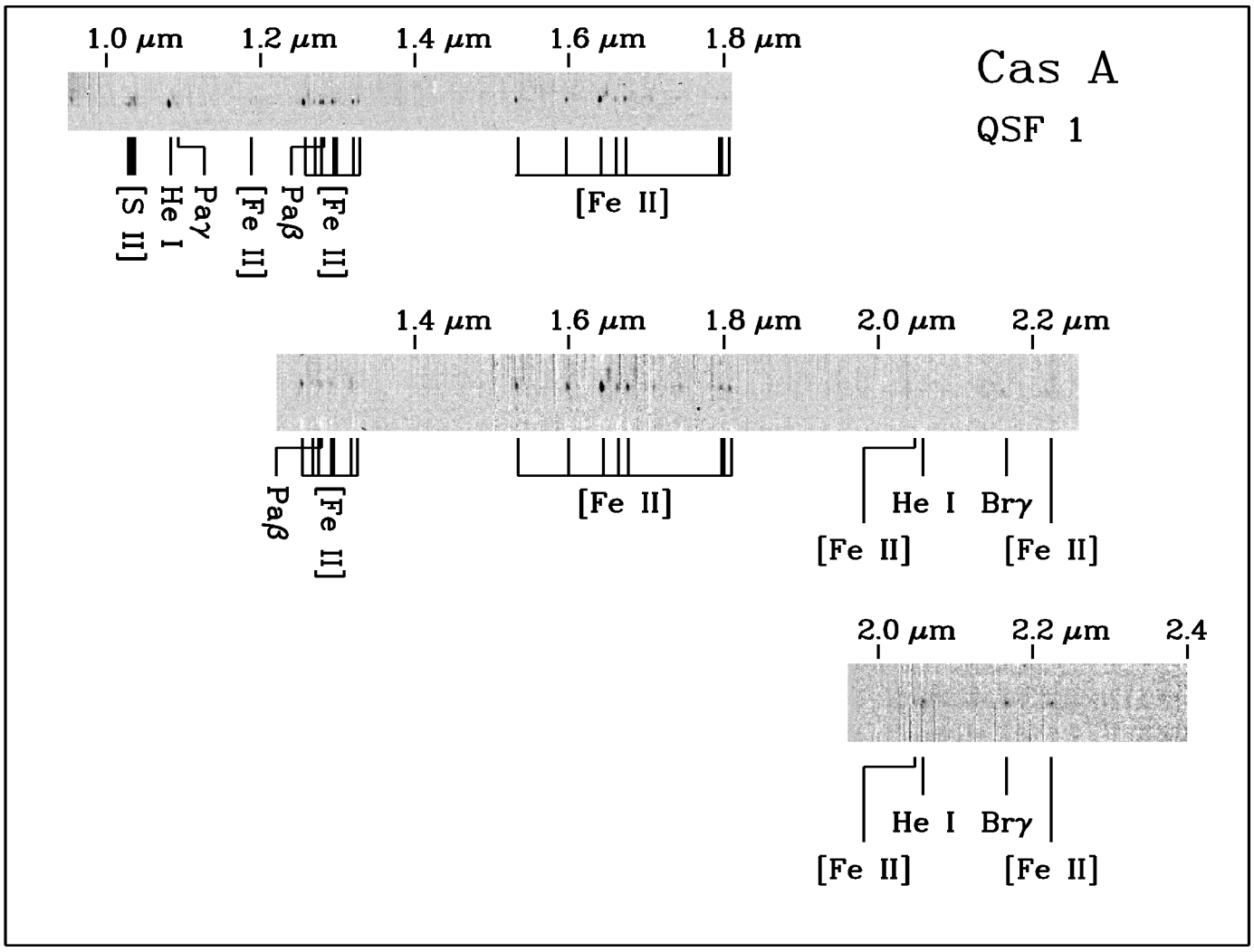


FIG. 4.—Two-dimensional long-slit spectra of QSF 1 in Cas A. [S II] and [Fe II] emission from a faint FMK can be seen just above the QSF spectrum.

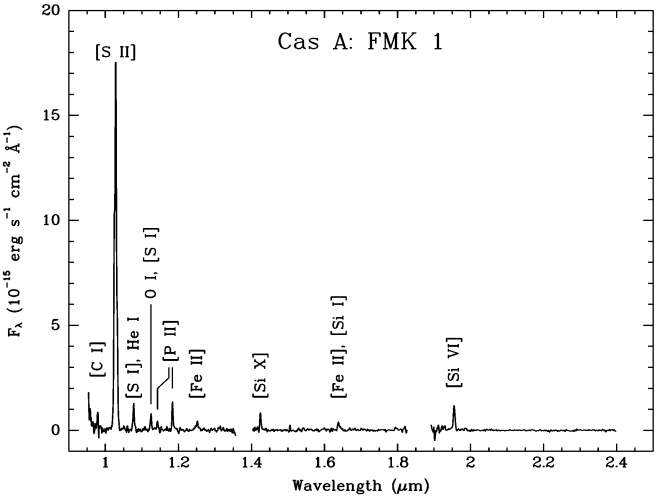


FIG. 5.—Observed NIR spectrum of FMK 1 in Cas A. The spectrum is dominated by strong [S II] emission but also exhibits a number of other faint lines, including [C I], [P II], and [Fe II], and high-ionization lines of [Si VI] and [Si X].

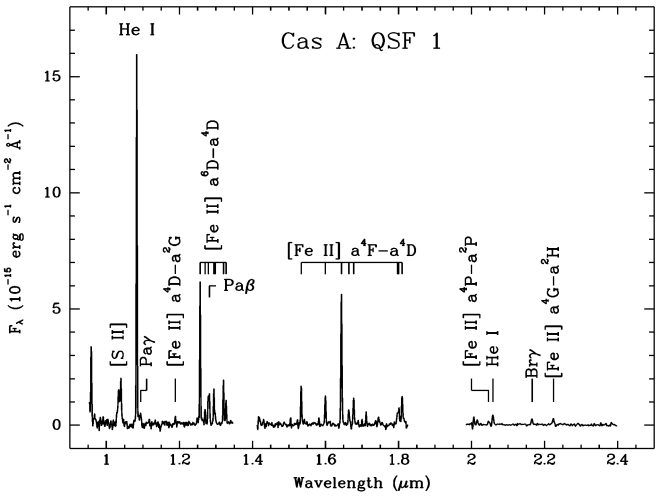


FIG. 6.—Observed NIR spectrum of QSF 1 in Cas A. The spectrum is dominated by strong He I 1.083 μm and [Fe II] emission lines.

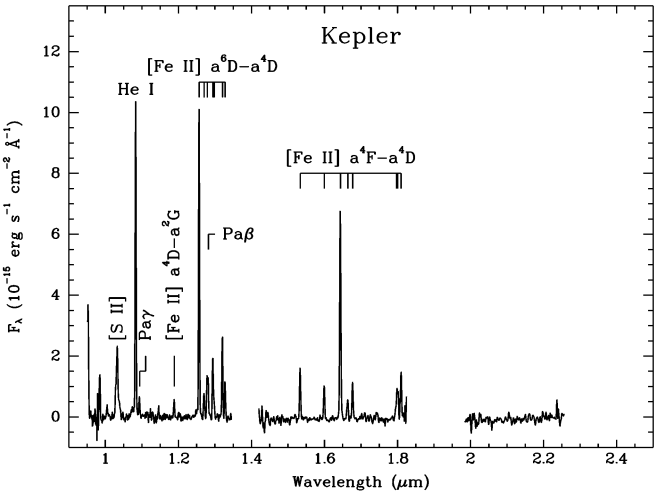


FIG. 7.—Observed NIR spectrum of a bright circumstellar knot on the west rim of Kepler's SNR. The spectrum is dominated by strong He I 1.083 μm and [Fe II] emission lines.

optical or near-infrared spectra of Cas A. However, we could find no other likely line identifications that fit the observed wavelengths. There are weak H_2 transitions at wavelengths near both lines, but we find no evidence of emission present from the much stronger H_2 feature at 2.12 μm. Also, the observed Doppler shifts of these lines, if identified as [Si VI] and [Si X], are consistent with each other and match those of the other lines seen in the FMKs to within the resolution of our data ($\approx$450 km s^{-1}). The absence of these lines in the spectra of the fainter FMKs is not significant as both of these lines suffer moderate telluric absorption and they could be too weak to detect in these fainter knots.

This is the first detection of these high-ionization silicon features in the spectrum of a supernova remnant. OMD90 looked for but did not detect [Si VI] in their spectra of RCW 103. However, the [Si VI] 1.965 μm line has been seen in planetary nebulae (Ashley & Hyland 1988), and both the [Si VI] 1.965 and [Si X] 1.4305 μm lines have been reported in NIR spectra of the solar corona (Münch, Neugebauer, & McCammon 1967), novae (Benjamin & Dinerstein 1990; Greenhouse et al. 1990), and AGNs (Oliva & Moorwood 1990; Thompson 1996; Murphy et al. 2000). Another high-ionization silicon line, [Si VII] 2.48 μm, has also been observed in many of these objects, but this line was outside the observed bandpass of the Cas A spectra shown here. However, in follow-up observations made in 2000 November this line was detected in 1.4–2.5 μm spectra of FMKs 1 and 2.

NIR spectra of novae often show other strong high-ionization features such as [S IX] 1.252, [S IX] 1.392, [Cr XI] 1.550, [P VIII] 1.736, [Al IX] 2.040, and [Ca VIII] 2.323 μm (Wagner & DePoy 1996), none of which are seen in our Cas

TABLE 4

LINE IDENTIFICATIONS FOR CAS A QSFS AND KEPLER SNR

λ_{rest} (μm)	LINE ID	CAS A QSF 1		CAS A QSF 2		CAS A QSF 3		KEPLER	
		$I(\lambda)$	$F(\lambda)$[a]	$I(\lambda)$	$F(\lambda)$[a]	$I(\lambda)$	$F(\lambda)$[a]	$I(\lambda)$	$F(\lambda)$[b]
0.9827, 0.9853	[C I] $^3P_{1,2}$–$^1D_2$	...	...	44	253	36	220	49	145
1.0290, 1.0323, 1.0339, 1.0373	[S II] $^2D_{5/2,3/2}$–$^2P_{3/2,1/2}$	111	595	[c]	[c]	104	534	157	423
1.0832	He I $^3S_1$–$^3P_{0,1,2}$	450	2060	607	2780	276	1260	340	848
1.0941	H I Paγ	16	71	14	65	9	37	17	42
1.1885	[Fe II] $a^4D_{7/2}$–$a^2G_{7/2}$	12	45	...	...	20	72	18	42
1.2570	[Fe II] $a^6D_{9/2}$–$a^4D_{7/2}$	173	572	95	315	211	700	329	675
1.2707	[Fe II] $a^6D_{1/2}$–$a^4D_{1/2}$	27	83	17	61	37	120	31	63
1.2791	[Fe II] $a^6D_{3/2}$–$a^4D_{3/2}$	85	269	65	210	78	250	79	160
1.2822	H I Paβ	...	...	...	...	...	...	...	...
1.2946	[Fe II] $a^6D_{5/2}$–$a^4D_{5/2}$	60	185	39	118	70	218	82	162
1.2981	[Fe II] $a^6D_{1/2}$–$a^4D_{3/2}$	...	...	...	...	...	...	...	...
1.3209	[Fe II] $a^6D_{7/2}$–$a^4{}_{7/2}$	58	176	28	83	75	226	84	172
1.3281	[Fe II] $a^6D_{3/2}$–$a^4D_{5/2}$	32	97	28	87	36	107	35	72
1.5339	[Fe II] $a^4F_{9/2}$–$a^4D_{5/2}$	58	138	17	38	79	187	61	105
1.5999	[Fe II] $a^4F_{7/2}$–$a^4D_{3/2}$	46	104	12	27	67	151	44	71
1.6440	[Fe II] $a^4F_{9/2}$–$a^4D_{7/2}$	203	440	57	125	288	628	273	432
1.6642	[Fe II] $a^4F_{5/2}$–$a^4D_{1/2}$	28	61	...	...	39	80	29	45
1.6773	[Fe II] $a^4F_{7/2}$–$a^4D_{5/2}$	44	93	18	44	63	134	45	69
1.7976	[Fe II] $a^4F_{3/2}$–$a^4D_{3/2}$	54	108	14	27	68	134	70	99
1.8005	[Fe II] $a^4F_{5/2}$–$a^4D_{5/2}$	...	...	...	...	...	...	...	...
1.8099	[Fe II] $a^4F_{7/2}$–$a^4D_{7/2}$	59	109	30	53	109	211	57	91
2.0466	[Fe II] $a^4P_{5/2}$–$a^2P_{3/2}$	9	16	...	...	7	12	...	...
2.0587	He I $^1S_0$–$^3P_1$	20	35	8	13	13	22	...	...
2.1661	H I Brγ	12	20	5	8	9	16	...	...
2.2244	[Fe II] $a^4G_{9/2}$–$a^2H_{11/2}$	15	23	5	8	8	12	...	...

NOTE.—Line fluxes are in units of 10^{-15} erg s^{-1} cm^{-2}.

[a] Corrected for $E(B-V) = 1.5$.

[b] Corrected for $E(B-V) = 0.9$.

[c] Blended with FMK.

A data. (Note that [S IX] 1.252 μm would be blended with [Fe II] 1.257 μm, and [S IX] 1.392 μm is obscured by strong telluric absorption). On the other hand, in near-infrared AGN spectra the [Si VI], [Si VII], and [Si X] lines are often the only strong high-ionization features seen in the 0.95–2.5 μm region.

Near-infrared "coronal" line emission in novae, AGNs, and planetary nebulae is believed to be due to photoionization, although collisional ionization from hot, shocked gas often cannot be ruled out. In contrast, the low-ionization optical spectra of Cas A's FMK knots have been modeled as shocks with a photoionized precursor component (Sutherland & Dopita 1995; HF96). Observed ratios of lines at different ionization levels are explained in these models as a mixture of emission from the rapidly cooling postshock region and from a precursor in the ejecta out ahead of the reverse shock, which is photoionized by UV emission from the shock front. Unfortunately, no predictions for [Si VI] and [Si X] emission have been made, so it is unclear whether the shock or precursor models can explain these very high-ionization lines. Alternatively, the high-ionization emission might be understood with a pure photoionization model such as those used to explain the high-ionization lines seen in novae, AGNs, and planetary nebulae. The main shell of Cas A is quite bright in X-rays (Hughes et al. 2000; Hwang, Holt, & Petre 2000), which could provide a strong photoionizing source.

In any case, it also seems likely that abundances play some role in the detection of these high-ionization silicon lines. Spectral modeling of optical FMK spectra indicate significant enrichment of metal abundances, suggesting that FMKs are gas from the inner regions of the exploded star (Chevalier & Kirshner 1979, HF96). Furthermore, X-ray imaging of Cas A has detected bright silicon line emission from the main shell ejecta (Hwang et al. 2000). All this indicates that the FMKs are likely silicon-rich and so it may be that only a small fraction of the silicon is highly ionized, with the bulk of the gas in a much lower ionization state. However, without a detailed spectral model it is impossible to conclude that the detection of these silicon lines is merely an abundance effect, as these lines are also detected in AGNs and planetary nebulae in which the silicon abundance is much lower. In fact, with respect to the observed high-ionization lines the Cas A spectra more closely resemble near-infrared AGN spectra than NIR spectra of novae, even though the gas in novae is probably closer in composition to the FMKs.

3.2. *Cas A QSFs and Kepler*

The optical spectra of shocked circumstellar knots in Cas A (QSFs) and Kepler's SNR are dominated by strong [N II] emission, with only a few other weak lines of H and He. These knots are thought to be nitrogen-enriched material shed by the progenitor star prior to the explosion and then shocked by the expanding blast wave (Peimbert & van den Bergh 1971). The NIR spectra of these knots seem consis?pm :SS:12.2: > tent with this picture, exhibiting an ISM-like spectrum with the strong [Fe II] emission typical of shocked gas. The Cas A QSFs and the Kepler knot are relatively bright in the near-infrared, especially in the J ($\sim$1.2 μm) and H ($\sim$1.6 μm) bands because of this rich [Fe II] spectrum. In addition to the [Fe II] lines, these circumstellar knots also show strong He I 1.083 μm emission, as well as the [S II] 1.03 μm blend, [C I] 0.9827, 0.9853, and He I 2.058 μm, and faint hydrogen lines (Paγ 1.0941, Paβ 1.2822, and Brγ 2.1661 μm). In fact, our QSF and Kepler spectra resemble the 1.4–2.4 μm spectrum of the optically brightest region of RCW 103 presented by OMD90 except that no H_2 emission was seen.

Several of the observed [Fe II] line ratios can be used as density diagnostics (e.g., Nussbaumer & Storey 1980; OMD89; OMD90). Using the dereddened ratios of the 1.5339, 1.5999, and 1.6642 μm lines to the strong 1.6440 μm line and the predicted ratios of OMD90, we estimated electron densities for each of the three QSFs in Cas A and for the Kepler knot. The results are shown in Table 5. In each case, the various line ratios all gave consistent estimates of the electron density for a given knot. The dereddened line ratios in each of the three QSFs observed in Cas A are indistinguishable to within the measurement errors and yield electron densities of $(5–9) \times 10^4$ cm^{-3}, which approach the high-density limit of the [Fe II] lines.

The density of the Kepler knot is roughly half that measured in the Cas A QSFs, namely, 2.5–3.1 $\times$ 10^4 cm^{-3}. Our estimate for the density of Kepler is somewhat higher than that measured at roughly the same position by OMD89, although it might be consistent with their upper limit. Differences in density estimates are not unexpected as OMD89 used a larger aperture (5.″8 $\times$ 5.″9 vs. our 0.″6 slit) and therefore sampled a much larger region of the remnant's northwest emission filaments.

Although electron densities in the three observed Cas A QSFs are similar, the He I to [Fe II] emission ratio varies dramatically. This is seen in Figure 8, which shows the observed NIR spectra of QSF 2 and QSF 3. In QSF 2, the He I 1.083 μm line is much brighter than the brightest [Fe II] lines, while in QSF 3, these lines are of nearly equal strength. Table 5 lists the dereddened He I 1.083 to [Fe II] 1.257 μm line ratio, which varies by nearly a factor of 5 in the three QSFs observed in Cas A. The observed variation could be due to temperature effects or compositional differences in the knots, for instance, in the depletion of gaseous iron into dust grains.

TABLE 5

CAS A QSF AND KEPLER: KNOT DENSITIES AND HE I/[FE II] FLUX RATIOS

Knot	[Fe II] λ1.5339 / [Fe II] λ1.6440	[Fe II] λ1.5999 / [Fe II] λ1.6440	[Fe II] λ1.6642 / [Fe II] λ1.6440	n_e (10^4 cm^{-3})	[He I] λ1.0832 / [Fe II] λ1.2570
Cas A QSF 1.....	0.314 $\pm$ 0.015	0.236 $\pm$ 0.015	0.139 $\pm$ 0.015	6.0–8.7	3.6 $\pm$ 0.2
Cas A QSF 2.....	0.304 $\pm$ 0.040	0.216 $\pm$ 0.040	...	3.2–8.9	8.8 $\pm$ 0.4
Cas A QSF 3.....	0.298 $\pm$ 0.010	0.240 $\pm$ 0.010	0.127 $\pm$ 0.010	5.2–6.9	1.8 $\pm$ 0.1
Kepler SNR	0.243 $\pm$ 0.015	0.164 $\pm$ 0.015	0.104 $\pm$ 0.015	2.5–3.1	1.3 $\pm$ 0.1

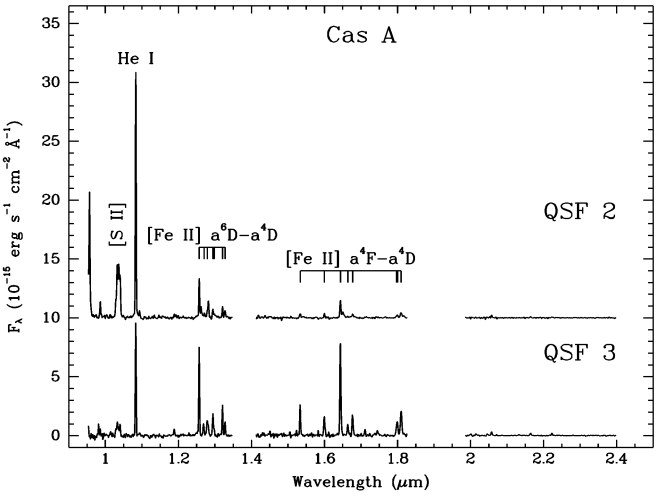


FIG. 8.—Observed NIR spectrum of QSF 2 and QSF 3 in Cas A, showing the large variation of the He I/[Fe II] emission ratio seen in the Cas A QSF data. The QSF 2 data have been shifted vertically by 10 units for clarity.

3.3. *J- and K-Band Images of Cas A*

J- and *K*-band mosaic images of Cas A are presented in Figures 9 and 10, respectively. In both images, the brightest emission comes from the QSFs. In *J*-band, this emission is almost entirely due to strong [Fe II] lines, while the *K*-band emission is a mixture of [Fe II], He I, and Brγ. The relative brightness of the QSFs in the two bands (i.e., the $J-K$ color) changes from knot to knot, and the NIR luminosity is poorly correlated with the optical luminosity. This may be related to the large variation of the observed He I 1.083 to [Fe II] 1.257 μm line ratio seen in the NIR spectra of the QSFs.

The FMK ejecta knots are also clearly visible in the *J*-band image. In this case, the emission is a mixture of weak [Fe II] and [P II] emission lines. Some FMK filaments are also visible in the *K*-band image, particularly in the inner regions of the remnant. The spectra of the bright northern FMKs showed no emission in *K* band, but the [Si VI] 1.96 μm line lies at the blue edge of the *K*-band filter. Thus the *K*-band filter may be picking up [Si VI] emission from fila-

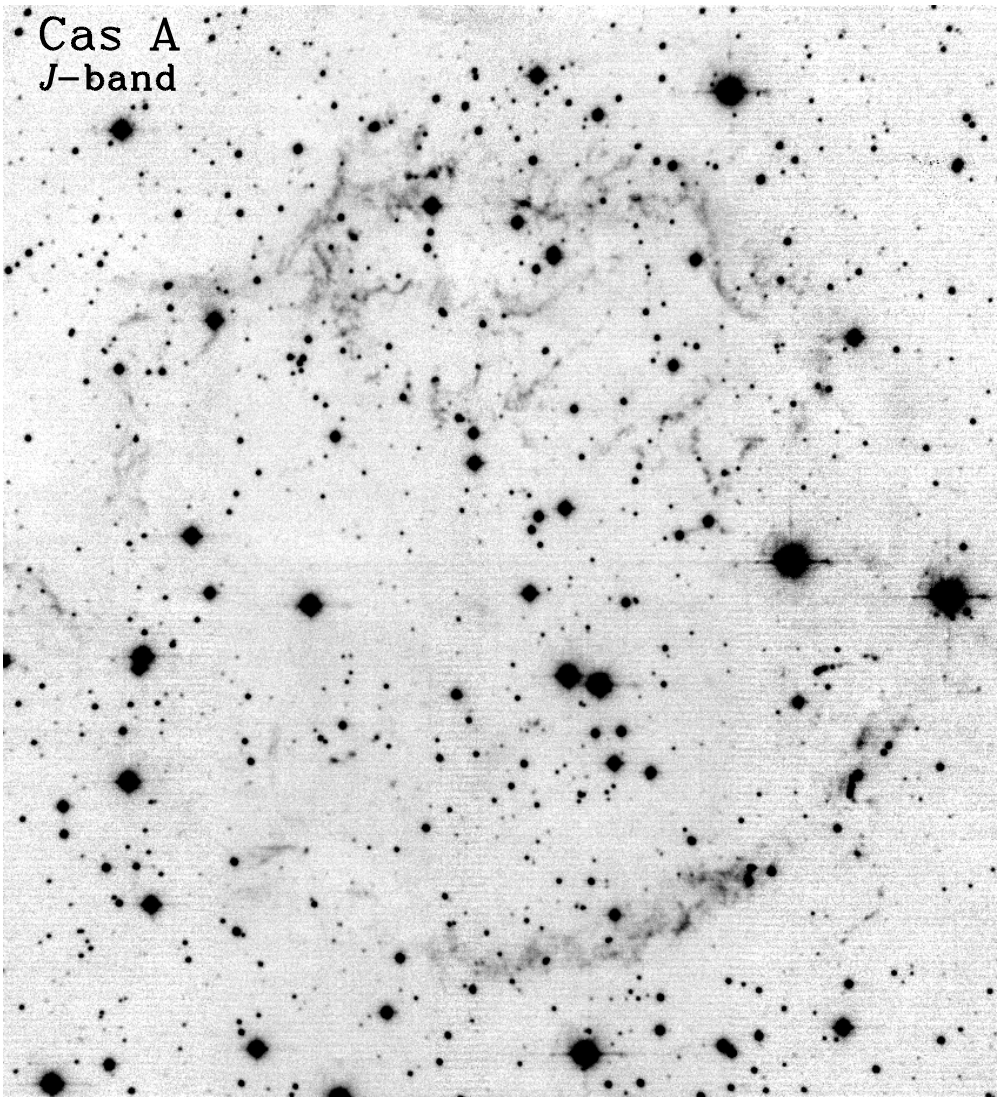


FIG. 9.—*J*-band image of Cas A. North is up and east is to the left. The *J*-band image is similar to optical images of Cas A with both circumstellar knots (QSFs) and ejecta knots (FMKs) clearly visible. Diffuse emission is also faintly detected in the *J* band near the center of the remnant and around the rim to the north and west.

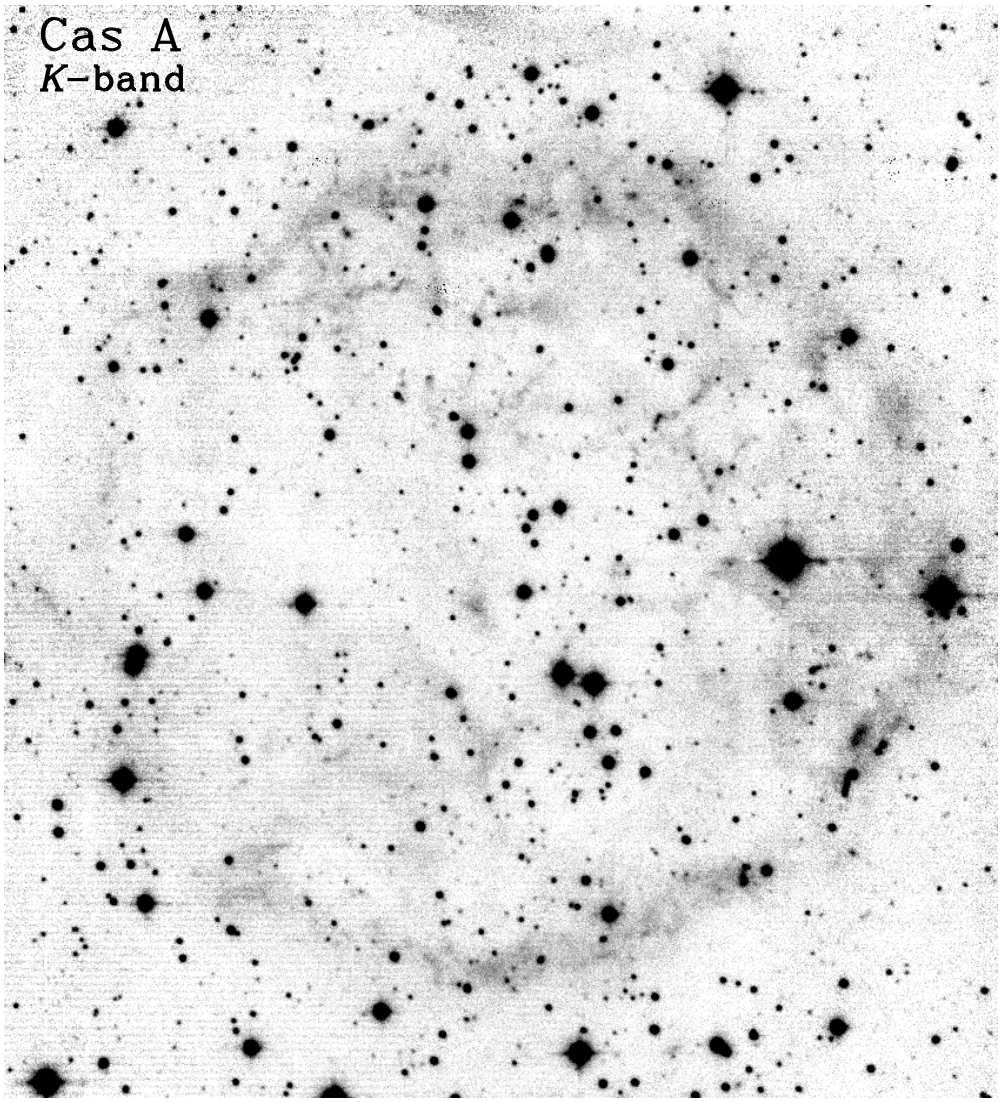


FIG. 10.—*K*-band image of Cas A. North is up and east is to the left. The dominant feature is diffuse emission that forms a nearly complete ring. The diffuse emission exhibits morphological similarities to radio continuum maps of Cas A.

ments with large positive radial velocities. This is supported by the fact that the filamentary emission in *K*-band largely disappears near the rim of Cas A and is seen primarily in the inner regions of the remnant where the radial velocities are largest.

The dominant feature in the *K*-band image is diffuse emission that forms a nearly complete ring around the rim of Cas A and also fills some of the interior. This diffuse emission can be faintly seen in the *J*-band image near the center and at several positions on the rim. This diffuse emission has no optical counterpart and does not correspond well to X-ray or mid-IR images of Cas A, either (cf. HF96; Lagage et al. 1996), but it does exhibit morphological similarities to radio continuum images (e.g., Anderson & Rudnick 1995). Some hint of the morphological differences between *K* band and optical images has been seen in the 2MASS images of Cas A.[2]

The lack of any detected diffuse line emission in the two-dimensional spectra of FMKs and QSFs on the rim (specifically FMKs 1 and 2 and QSFs 1 and 2) suggest that the diffuse emission is continuum rather than line emission. The large morphological differences between the *K*-band and mid-IR images and the detection of the diffuse emission in *J* band argue against thermal dust emission as a source. The thermal dust emission seen in the mid-infrared is well correlated with the optical knots (Lagage et al. 1996), and the detection of thermal emission in *J* band would probably require prohibitively high dust temperatures at or above typical grain destruction limits. On the other hand, the morphological similarity of the diffuse emission with radio continuum images suggests that the diffuse *K*-band emission may be infrared synchrotron radiation.

4. CONCLUSION

We have presented the first near-infrared (NIR) spectra of a young metal-rich supernova remnant. The spectra of fast-moving ejecta knots in Cas A are dominated by [S II] 1.03 μm emission but show several other faint emission lines, including high-ionization lines of [Si VI] and [Si X]. These forbidden silicon lines have often been seen in NIR spectra of novae and AGNs but have never before been detected in

[2] See http://www.ipac.caltech.edu/2mass/gallery/powarc8.html.

a supernova remnant. Interestingly, the silicon lines represent a much higher ionization state than the observed optical and near-infrared emission lines. Therefore, further study of the spatial distribution of the [Si VI] and [Si X] line emission may provide valuable information about the ionization structure in the metal-rich Cas A ejecta.

We also obtained NIR spectra of shocked circumstellar knots in Cas A and Kepler, which are shown to have bright He I and [Fe II] emission. Analysis of relative [Fe II] line ratios indicate electron densities $\sim 10^4$–10^5 cm^{-3} in these knots. While the measured density was relatively constant for the three circumstellar knots observed in Cas A, the He I/[Fe II] emission ratios were found to vary by nearly a factor of 5.

Finally, we presented J- and K-band images of Cas A. While the J-band image is largely similar to optical images, the dominant feature in the K band is diffuse emission that best matches radio continuum images of Cas A and may be near-infrared synchrotron emission.

We would like to thank Bob Barr and the MDM staff for their excellent assistance in instrument setup and general observing support. This research is supported by NSF grant 98-76703.

REFERENCES

Anderson, M. C., & Rudnick L. 1995, ApJ, 441, 307
Ashley, M. C. B., & Hyland, A. R. 1988, ApJ, 331, 532
Benjamin, R. A., & Dinerstein, H. L. 1990, AJ, 100, 1588
Blair, W. P., Long, K. S., & Vancura, O. 1991, ApJ, 366, 484
Burton, M., & Spyromilio, J. 1993, Proc. Astron. Soc. Australia, 10, 327
Cardelli, J. A., Clayton, G. C., & Mathis, J. S. 1989, ApJ, 345, 245
Chevalier, R. A., & Kirshner, R. P. 1979, ApJ, 233, 154
Dennefeld, M. 1982, A&A, 112, 215
Dennefeld, M., & Andrillat, Y. 1981, A&A, 103, 44
Fesen, R. A., & Hurford, A. P. 1996, ApJS, 106, 563
Graham, J. R., Wright, G. S., & Geballe, T. R. 1991, ApJ, 372, L21
Graham, J. R., Wright, G. S., Hester, J. J., & Longmore, A. J. 1991, AJ, 101, 175
Graham, J. R., Wright, G. S., & Longmore, A. J. 1987, ApJ, 313, 847
———. 1990, ApJ, 352, 172
Greenhouse, M. A., Grasdalen, G. L., Woodward, C. E., Benson, J., Gehrz, R. D., Rosenthal, E., & Skrutskie, M. F. 1990, ApJ, 352, 307
Greenhouse, M. A., et al. 1997, ApJ, 476, 105
Hanson, M. M., Conti, P. S., & Rieke, M. J. 1996, ApJS, 107, 281
Hanson, M. M., Rieke, G. H., & Luhman, K. L. 1998, AJ, 116, 1915 (HRL98)
Henry, R. B. C., MacAlpine, G. M., & Kirshner, R. P. 1984, ApJ, 278, 619
Hoffleit, D., & Jaschek, C. 1982, The Bright Star Catalog (4th. ed.; New Haven: Yale Univ. Obs.)
Hughes, J. P., Rakowski, C. E., Burrows, D. N., & Slane, P. O. 2000, ApJ, 528, L109
Hurford, A. P., & Fesen, R. A. 1996, ApJ, 469, 246 (HF96)
Hwang, U., Holt, S. S., & Petre, R. 2000, ApJ, 537, L119
Kurucz, R. L. 1994, CD-ROM 19, Solar Abundance Model Atmospheres for 0, 1, 2, 4, 8 km/s (Cambridge: Smithsonian Astrophys. Obs.)
Lagage, P. O., Claret, A., Ballet, J., Boulanger, F., Cesarsky, C. J., Cesarsky, D., Fransson, C., & Pollock, A. 1996, A&A, 315, L273
Livingston, W., & Wallace, L. 1991, NSO Tech. Rep. 91-001 (July)
Massey, P., & Gronwall, C. 1990, ApJ, 358, 344
Münch, G., Neugebauer, G., & McCammon, D. 1967, ApJ, 149, 681
Murphy, T. W., Jr., Soifer, B. T., Matthews, K., & Armus, L. 2000, AJ, 120, 1675
Nussbaumer, H., & Storey, P. J. 1980, A&A, 89, 308
Oliva, E., & Moorwood, A. F. M. 1990, ApJ, 348, L5
Oliva, E., Moorwood, A. F. M., & Danziger, I. J. 1989, A&A, 214, 307 (OMD89)
———. 1990, A&A, 240, 453 (OMD90)
Peimbert M., & van den Bergh, S. 1971, ApJ, 167, 223
Richter, M. J., Graham, J. R., & Wright, G. S. 1995, ApJ, 454, 277
Rudy, R. J., Rossano, G. S., & Puetter, R. C. 1994, ApJ, 426, 646
Seward, F. D., Harnden, F. R., Jr., Murdin, P., & Clark, D. H. 1983, ApJ, 267, 698
Sutherland, R. S., & Dopita, M. A. 1995, ApJ, 439, 381
Thompson, R. I. 1996, ApJ, 459, L61
Treffers, R. R. 1979, ApJ, 233, L17
Wagner, R. M., & DePoy, D. L. 1996, ApJ, 467, 860
Wallace, L., Hinkle, K., & Livingston, W. 1993, NSO Tech. Rep. 93-001 (April)